Surface freezing in binary alkane-alcohol mixtures

E. Ofer,[1] E. Sloutskin,[1] L. Tamam,[1] B. M. Ocko,[2] and M. Deutsch[1,*]
[1]*Department of Physics, Bar-Ilan University, Ramat-Gan 52900, Israel*
[2]*Department of Condensed Matter Physics and Materials Science, Brookhaven National Laboratory, Upton, New York 11973, USA*
(Received 12 May 2006; published 7 August 2006)

Surface freezing was detected and studied in mixtures of alcohol and alkane molecules, using surface tensiometry and surface-specific x-ray scattering methods. Considering that surface freezing in pure alkanes forms an ordered monolayer and in alcohols it forms an ordered bilayer, the length mismatch repulsion was minimized by varying the carbon number of the alkane component around $2n$, where n is the carbon number of the alcohol molecule. A solutionlike behavior was found for all mixtures, where the ideal liquid mixture phase-separates upon freezing both in the bulk and the surface. The solid exhibits a herringbone crystalline phase below an alkane mole fraction $\phi_t \approx 0.8$ and a rotator phase above it. The surface frozen film below ϕ_t is an alkane monolayer exhibiting a next-nearest neighbor molecular tilt of a composition-dependent magnitude. Above ϕ_t, no diffraction peaks were observed. This could be explained by the intrinsically shorter-range order of the rotator phase and a possible proliferation of defects.

DOI: 10.1103/PhysRevE.74.021602 PACS number(s): 68.03.Hj, 61.10.Kw, 61.25.Hq

I. INTRODUCTION

The surface freezing (SF) effect is the formation of a solid quasi-two-dimensional (2D) layer at the surface of a melt at a temperature (T_s) higher than its bulk freezing temperature (T_b) [1–4]. This phenomenon somewhat contrasts intuition, as the surface molecules are usually considered to have higher entropy than the bulk molecules, leading one to expect the opposite effect, surface melting—the formation of a liquid layer at the solid-vapor interface below the bulk freezing temperature. Indeed, surface melting has been observed in metals, semiconductors, polymers, ice, and molecular crystals [5]. By contrast, surface freezing has been observed so far almost exclusively in chain molecules, where it was originally discovered over a decade ago [1–4,6]. In these molecules, however, it seems to be the rule rather than the exception: SF was observed in alkanes and their mixtures, alkenes, semifluorinated alkanes, alcohols and their mixtures, alkyl-oligo-ethyleneglycols, and α,β-diols [1–4,7–12]. Moreover, as chain molecules are among the fundamental building blocks of many, more complex, molecules it is conceivable that their properties, including surface freezing, will be reflected in the properties and behavior of their host molecules. Indeed, the SF effect was found to occur in long "hairy" polymers with alkyl side chain [13] and even in much more complex biological systems such as the Bacteriophage fd virus [14]. Recent studies focus on the elastic properties of the surface-frozen layer [15] and on the layer's influence on the near-surface hydrodynamics [16].

Normal alkanes [$CH_3(CH_2)_{n-2}CH_3$ denoted in the following as C_n] and their mixtures are nonpolar. Thus, the only forces present in melts and solids of these molecules are van der Waals (vdW) forces, and only a single surface-frozen monolayer is formed over the melt [3,11]. However, alcohols [$CH_3(CH_2)_{n-1}OH$ denoted as C_nOH] comprise a hydroxyl end group which gives rise to hydrogen bonds (HB) in addition to vdW forces. These interactions result in the surface-frozen layer of alcohols being a bilayer with the hydroxyl group residing at the bilayer's center. This occurs in both monocomponent alcohol melts and in binary alcohol mixtures [4,12]. For binary mixtures of different-length, same-species molecules, the surface and bulk phase diagrams were both well accounted for using the standard thermodynamics of mixtures [17,18], treating the liquid phase as an ideal mixture, and the solid phase as a strictly regular mixture [10,11]. Thus, for different-length molecules of the same species the free energy of the crystalline phase is controlled by the repulsion between adjacent molecules of mismatched lengths [11,12,19]. This repulsion energy is determined by the interchange parameter ω, which is the energy change upon replacing one molecule of the pure phase of one species by a molecule of the other species [17]. ω played a crucial role in determining the phase diagrams of both the bulk and the surface in binary alcohol-alcohol [12] and alkane-alkane [11] binary mixtures. Moreover, ω was found to exhibit a universal behavior in both bulk and surface, depending only on the square of the reduced chain length mismatch $\Delta n/\bar{n}$, where Δn and $\bar{n}$ are, respectively, the difference in and average of the number of carbons of the two components [19].

The fact that both alkane mixtures and alcohol mixtures show the same phase behavior, with the same universal ω, indicates that the moiety common to both molecules, the alkyl chains, dominates the behavior induced by mixing, beyond the intrinsic behavior of the pure components. The hydrophobic repulsion of the hydroxyl groups from the alkyl chains, present in the alcohol mixtures but absent in the alkane mixtures, does not seem to play a significant role in the structure of the mixture beyond that of the pure alcohols. This, in turn, is most probably due to the fact that in the surface-frozen phase of alcohol mixtures, as well as in pure alcohols, the hydroxyl groups lie all within a single layer. Thus, no close hydroxyl-methyl contacts are formed between adjacent alcohol molecules.

The present study explores the influence of such close contacts, by employing alkane-alcohol mixtures. Here, a ho-

*Email address: deutsch@mail.biu.ac.il

mogeneously mixed surface-frozen layer of extended molecules will necessitate hydroxyl-methyl contacts between adjacent molecules, and add the corresponding repulsion term to the free energy. By varying the composition, i.e., the number of hydroxyl groups per alkane molecule, we tune the average strength of this repulsion from zero (100% alkane, 0% alcohol) up to a maximal value (0% alkane, 100% alcohol). We have chosen to study alkanes with a number of carbons m, which is roughly twice that of the alcohol, n: $m=2n+\Delta n$. Considering that in their surface-frozen phase alkanes form a monolayer while alcohols form a bilayer, this allowed us to tune the length-mismatch repulsion for a homogeneously mixed phase through, and around, zero by varying the length difference Δn through zero. The next section presents the experimental techniques, with the two subsequent ones discussing the results obtained from the surface tension and x-ray measurements, respectively. The last section presents the conclusions arising from these results.

II. EXPERIMENT

The thermodynamics of the surface was studied by surface-tension (ST) measurements [20]. The structure of the surface was studied by x-ray reflectivity (XR), grazing incidence diffraction (GID), and Bragg rod (BR) measurements, using a synchrotron-based liquid-surface diffractometer [21].

A. Samples and cells

The alkane and alcohol samples were purchased from Sigma-Fluka-Aldrich. The $C_{18}OH$ and the $C_{22}OH$ were labeled >98% pure and the C_{36}, C_{40}, and C_{44} were labeled >99% pure. All materials were used as received. The mixtures were prepared by weighing the required amount of each material in a copper cell, heating to ~10 °C above the highest melting point, and stirring by a magnetic stirrer at this temperature for approximately 30 min. The well-mixed sample was either kept in its copper container (for surface tension measurements) or poured onto a preheated copper substrate (for x-ray measurements). These were put into a two-stage oven, the outer shell of which was a passive aluminum cell and the inner shell was temperature controlled to 0.001 °C. The results of the measurements were observed to be independent of the thermal history of the sample, yielding the same results when cooled below the bulk freezing temperature and reheated. However, the results presented here are those obtained in the first cooling cycle of the liquid mixture, immediately after the preparation of the mixed sample.

B. Surface tension measurements

The ST measurements employed the Wilhelmy plate method [20]. Filter paper plates were used in order to enhance the wetting of the plate by the melt [10]. The plate is attached to an electronic balance, which measures the force applied by the surface to the plate. The surface tension is obtained by dividing this force by the plate's circumference. The samples were maintained in a temperature-regulated cell which is almost the same as that used in the x-ray measurements except for a small hole in its cover to pass the wire connecting the balance to the plate. The temperature of the liquid mixture was varied stepwise, at a rate of 0.03 °C/30 s.

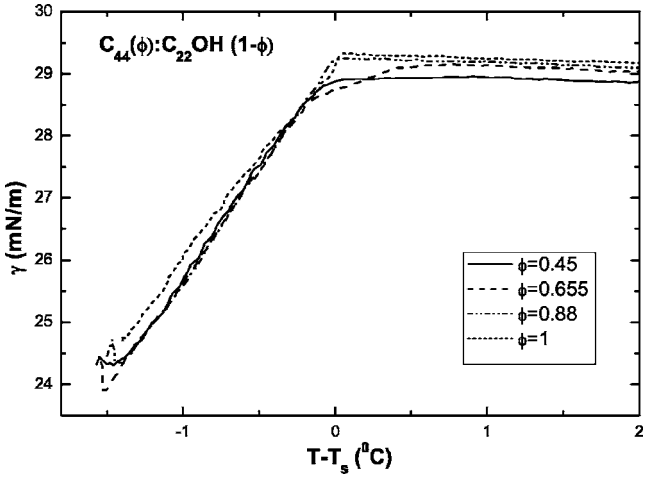

FIG. 1. Surface tension temperature scans of $C_{44}+C_{22}OH$ mixtures for the indicated liquid-bulk concentrations ϕ^b of C_{44}. The sharp change in the slope denotes the surface-freezing temperature T_s. The curves end at the bulk-freezing temperature T_b.

The surface tension γ is a direct measure of the excess free energy of the surface over that of the bulk: $\gamma=\epsilon^s-\epsilon^b-T(S^s-S^b)$. Here ϵ^s and ϵ^b are the energies and S^s and S^b are the entropies of the surface and bulk, respectively. The temperature slope of $\gamma(T)$ yields the surface excess entropy: $d\gamma/dT=-(S^s-S^b)$. For a liquid surface $S^s>S^b$ and $d\gamma/dT<0$. If the surface undergoes an ordering transition at some temperature, S^s becomes smaller than S^b and $d\gamma/dT>0$. Thus, the signature of an order-disorder transition at the surface is an abrupt change in the sign of $d\gamma/dT$. Surface freezing is such a transition and is observed in a $\gamma(T)$ measurement as a sharp slope change from a small negative value at $T>T_s$ to a large positive value for $T<T_s$ [3,10]. The measured $\gamma(T)$ curves shown in Fig. 1 for several $C_{44}+C_{22}OH$ mixtures clearly exhibit this effect [22].

Experimentally, the onset of bulk-freezing T_b is marked by the strong fluctuations it induces in the force that the sample exerts on the Wilhelmy plate. The surface excess entropy ΔS^s is obtained from the slope of the measured $\gamma(T)$. Note that this value is per unit area, as is γ, rather than per molecule [10]. The significance of this is discussed below.

C. X-ray measurements

1. X-ray reflectivity

X-ray reflectivity (XR) yields information on the electron-density profile normal to the surface, including the thickness and electron density of the surface-frozen layer [23]. The reflected beam is measured by placing the detector in the reflection plane at a detection angle β equal to the angle of incidence of the x-ray beam α. The reflectivity, defined as the ratio between incident and reflected intensities, is measured as a function of the wave-vector transfer normal to the sur-

face, $q_z=(4\pi/\lambda)\sin\alpha$ in the reflection plane [23,24]. $\lambda \approx 1.54$ Å is the wavelength of the synchrotron radiation used.

An ideally smooth and sharp liquid-vacuum interface yields the Fresnel reflectivity,

$$R_F(q_z) = \left| \frac{q_z - \sqrt{q_z^2 - q_c^2}}{q_z + \sqrt{q_z^2 - q_c^2}} \right|^2, \quad (1)$$

where $q_c=(4\pi/\lambda)\sin\alpha_c$, with the critical angle for total external reflection given by $\alpha_c \approx \sqrt{r_e \rho_e \lambda^2/\pi}$. r_e is the classical electron radius and ρ_e is the electron density of the bulk. We neglect absorption as it affects in our case only the near-α_c region, and even there its influence is quite minor.

When the liquid surface is covered by a layer with an electron density different from that of the bulk, the x rays reflected from the top and bottom of the layer interfere to produce Kiessig-type fringes in the reflectivity $R(q_z)$. The period of the fringes Δq_z is related to the layer thickness D by $\Delta q_z = 2\pi/D$. A more complex density profile can be approximated by $N+1$ uniform-density slabs, which yield (within the Born approximation, valid for $q_z \gtrsim 4q_c$ Ref. [25]), the expression

$$R(q_z)/R_F = \left| \sum_{j=0}^{N} \left(\frac{\rho_j - \rho_{j+1}}{\rho_0} \right) \exp^{-iq_z D_j} \exp^{-q_z^2 \sigma_{j+1}^2/2} \right|^2. \quad (2)$$

Here, D_j is the distance of the jth interface from the bulk, σ_j is its roughness, and ρ_j is the electron density of the jth slab. $\rho_0=\rho_{bulk}$ and $\rho_{N+1}\approx 0$ is the electron density of the vapor.

Equation (2) was used to analyze the XR data. For alkanes, $N=2$ was sufficient to yield a good fit to the measured curves. The same model was successfully used in the past to represent the surface-normal electron density profiles of surface-frozen alkane melts [2,3], binary alkane mixtures [11], and alkane-containing solutions [10]. In this model the upper slab represents the $(CH_2)_{n-2}$ alkyl chain and the lower slab represents the smaller-density CH_3 methyl group at the interface between the solid monolayer and the liquid bulk. The second methyl group, at the monolayer-vapor interface, is included in the roughness of the interface between the solid layer and the vapor. In this model it is assumed that all interfaces have the same roughness. Thus, the model includes five adjustable parameters: two thicknesses, two densities, and one roughness.

For alcohols, where a bilayer forms at the melt's surface upon surface freezing, a four-slab ($N=4$) model was used. This model was used successfully for alcohols (dry and hydrated) [4,7] and binary alcohol mixtures [12]. In this model the first and third slab are identical and represent the chain of the upper and lower $(CH_2)_{n-1}$ alkyl groups, respectively. The second slab represents the layer of OH head groups and the fourth slab represents the layer of CH_3 methyl groups at the bilayer-liquid bulk's interface. As in the case of the monolayer, the CH_3 methyl group at the bilayer-vapor interface is included in the interface roughness. In this model three roughnesses were assumed: (1) at the bilayer-vapor interface, (2) at the upper and lower interfaces of the OH slab, and (3) at the bilayer bulk-liquid interface. In both slab models an additional slab, of infinite thickness, represents the liquid subphase. Both of these models were used to analyze the reflectivity data measured for the binary alkane-alcohol mixtures in order to determine the surface-frozen structure.

2. Grazing incidence diffraction and Bragg rods

Grazing incidence x-ray diffraction measurements were used to probe the in-plane structure of the SF layer [23,26]. In these measurements $\alpha < \alpha_c$, the incident x-rays undergo total reflection and only evanescent waves penetrate the surface to a depth of approximately 100 Å. Scanning the detector angle θ_D out of the plane of the specular reflection enabled us to measure the scattered intensity as a function of the in-plane momentum transfer $q_r=(4\pi/\lambda)\sin(\theta_D/2)$ [3,23,26]. The GID patterns obtained were analyzed using standard crystallographic techniques [3,4]. The q_r positions of the peaks in the pattern yield information on the in-plane molecular packing. The widths of the peaks are inversely proportional to the crystalline coherence length within the sample. The surface-normal intensity distribution at the positions of the GID peaks, called Bragg rods (BR), yield information on the magnitude and azimuthal direction of the molecular tilt within the surface-frozen layer. A vertically oriented metal wire linear position sensitive detector (PSD) was employed to measure this distribution simultaneously for a range of q_z values.

As we show below, the surface-frozen layer of all mixtures studied here is a nearly pure monolayer of the alkane component of the mixture. In this case, the intensity distribution of the BR along the surface normal direction is well approximated by [3,4,26]

$$I(q_z) \propto \left(\frac{\sin(Q_z D/2)}{Q_z/2} \right)^2 (\exp^{-q_z^2\sigma^2}) |T(\alpha)|^2 |T(\beta)|^2. \quad (3)$$

Here $|T(\alpha)|^2 = |2\sin\alpha/(\sin\alpha + \sqrt{\cos^2\alpha_c - \cos^2\alpha})|^2$ is the surface enhancement factor for the incident beam and $|T(\beta)|^2$ is an equivalent term for the reflected beam [27]. The wave-vector transfer components along (normal to) the molecule's long axis, denoted Q_z (Q_r), and those along (normal to) the surface normal, denoted q_z (q_r), are related by

$$Q_z = q_z \cos\theta - q_x \sin\theta, \quad (4)$$

$$Q_r = \sqrt{q_y^2 + (q_z \sin\theta + q_x \cos\theta)^2}. \quad (5)$$

Here θ is the tilt angle of the molecule away from the surface normal [3,26,28] and q_x and q_y are the wave-vector transfers in the surface-parallel plane with the y axis lying in the reflection plane.

As detailed in Ref. [3], when molecules tilt in the next-nearest-neighbor direction and pack hexagonally in the molecule-normal plane, two GID peaks are observed at q_{r1} and $q_{r2} > q_{r1}$, respectively. At q_{r1} Eq. (3) peaks in the surface-normal q_z direction at some $q_{z1} \neq 0$, while for q_{r2} it peaks at $q_{z2}=2q_{z1}$. These are the signatures of a next-nearest-neighbor tilt, which are indeed observed in our case, as discussed below. For this packing, with two equivalent molecules per unit cell, the reflections (01) and (10) are forbidden, as are all (hk) reflections where $h+k$ is odd. The

lowest-order reflection is the (02), which is nondegenerate, while the next order is the twice-degenerate $(11)+(1\bar{1})$ reflection.

III. RESULTS: THERMODYNAMICS

The surface-tension measurements provided values for three thermodynamical quantities: the surface- and bulk-freezing temperatures T_s and T_b, respectively, and the entropy loss per unit area upon surface freezing ΔS^s, as a function of the bulk mole fraction ϕ^b of the alkane. These quantities, derived from the measured $\gamma(T)$ curves, are listed in Table I. These values, along with the known properties of the pure components, were used to determine the phase of the solid in the bulk and on the surface. We used three different theoretical approaches: (a) the liquid phase is treated as an ideal mixture, where the free energy includes, in addition to the free energies of each species, an entropic mixing term only. The solid phase is treated as a strictly regular mixture, where the free energy includes an additional repulsion term, proportional to the interchange parameter. This was the approach used for alkane-alkane [11] and alcohol-alcohol [12] mixtures in previous studies. (b) Both liquid and solid phases are treated as strictly-regular mixtures with different interchange parameters for the liquid and the bulk. (c) A solution behavior is assumed: the liquid phase is treated as an ideal mixture, and assumed to phase separate upon freezing. The solid phase is treated, therefore, as a pure, unmixed, phase. There is no mixing term in the free energy in this phase.

A. Results for the bulk

Using the equality of the chemical potentials of the solid and liquid at the freezing temperature T_b with Eqs. (A2) and (A3) as detailed in the Appendix, we obtain for approach (a) above,

$$T_b(\phi^b) = [T_{b,n}\Delta S_n^b - \omega_{cb}(1-x_b)^2]/\{\Delta S_n^b + k_B \ln(x_b/\phi^b)\}, \tag{6}$$

$$T_b(\phi^b) = (T_{b,m}\Delta S_m^b - \omega_{cb}x_b^2)/\{\Delta S_m^b + k_B \ln[(1-x_b)/(1-\phi^b)]\}. \tag{7}$$

Here the superscript and subscript b denotes the bulk; x_b is the mole fraction of component n in the frozen phase and ω_{cb} is the interchange parameter in the crystalline bulk phase. Using values of the entropy loss upon bulk freezing ΔS_i^b and the bulk freezing temperatures T_b of the pure components, $i=n,m$ from previous measurements [3,4,29], Eqs. (6) and (7) can be solved by fitting them to the $T_b(\phi^b)$ values measured here for a given liquid mixture. These fits yield the interchange parameter ω_{cb}, which upon substitution into Eqs. (6) and (7), yields the solid bulk concentration x_b. Equations (6) and (7) were found to fit the measured T_b values poorly for a finite ω_{cb} for all mixtures studied here. An infinite ω_{cb}, or rather $\omega_{cb} \gg k_B T$, means that the repulsion term is much larger than the entropic mixing term. This, in turn, implies that phase separation should occur upon freezing, and the system is better described as a solution.

Approach (b) adds one more parameter, the liquid phase interchange energy ω_{lb} and the equations corresponding to Eqs. (6) and (7) become

TABLE I. Thermodynamical data derived from surface tension measurements.

ϕ^b	T_s (°C)	T_b (°C)	ΔS^s (mJ/[m^2 K])
	$C_{36}(\phi^b)+C_{18}OH(1-\phi^b)$		
0	57.5	57.1	2.0
0.09	57.4	56.9	2.8
0.248	64.5	63.8	3.6
0.319	66.3	64.9	3.5
0.445	68.7	67.4	3.3
0.502	69.6	68.4	2.9
0.555	70.2	69.1	3.5
0.652	71.8	70.6	2.3
0.738	72.8	71.2	2.2
0.814	74.2	72.1	2.0
0.882	75.1	72.9	2.1
1	77.6	75.4	2.1
	$C_{40}(\phi^b)+C_{18}OH(1-\phi^b)$		
0	57.6	57.1	1.8
0.099	62.1	61.7	1.9
0.188	66.8	65.9	3.3
0.342	72.1	70.7	4.0
0.410	73.4	71.9	3.4
0.472	74.6	73.1	3.9
0.581	75.9	74.5	3.8
0.676	77.3	76.2	3.5
0.757	78.3	77.1	3.6
0.829	79.5	77.9	3.1
0.892	80.6	78.7	2.5
0.949	81.5	79.7	2.4
1	82.9	80.6	2.4
	$C_{44}(\phi^b)+C_{22}OH(1-\phi^b)$		
0	70.2	69.5	2.2
0.174	71.8	71.1	3.1
0.322	76.9	76.1	2.7
0.448	79.9	78.4	3.6
0.558	81.0	79.6	3.4
0.655	82.2	80.6	3.2
0.699	82.5	81.2	3.7
0.74	83.3	81.6	3.2
0.816	83.9	82.4	3.3
0.883	84.4	83.2	3.7
0.944	85.7	84.1	3.1
1	86.6	85.2	3.3

$$T_b(\phi^b) = [T_{b,n}\Delta S_n^b + \omega_{lb}(1-\phi^b)^2 - \omega_{cb}(1-x_b)^2]/\{\Delta S_n^b + k_B \ln(x_b/\phi^b)\}, \quad (8)$$

$$T_b(\phi^b) = [T_{b,m}\Delta S_m^b + \omega_{lb}(\phi^b)^2 - \omega_{cb}x_b^2]/\{\Delta S_m^b + k_B \ln[(1-x_b)/(1-\phi^b)]\}. \quad (9)$$

Solving these equations, as above, by fits to the measured $T_b(\phi^b)$, yields good fits only when $\omega_{cb} \to \infty$. This indicates a dominance of the repulsion term, so that the liquid mixture behaves as a solution at the freezing point, rather than as a mixture. For all mixtures studied here, the pure alkane has a higher freezing temperature than that of the alcohol, and thus it is the alkane which freeze out at T_b. Indeed, good fits were obtained only when the entropy change ΔS_b was that of the liquid-to-rotator transition of the alkane component of each liquid mixture. However, this also implies that the alkane freezes into a rotator phase, which is inconsistent with the transition temperatures of the various phases of the pure alkanes studied, as we now explain. Calorimetric studies [29] show that for pure C_{36} the liquid-to-rotator transition at 75.4 °C preempts an extrapolated liquid-to-crystal transition at 74.9 °C. A solid-solid rotator to crystal transition occurs at $T_{R\to C}$=73.6 °C. As seen in Table I, T_b for C_{36}+C_{18}OH mixtures are well below 73.6 °C for almost all mole fractions studied. Thus, for those ϕ^b at least, the freezing of the alkane in the liquid mixture must be into a crystalline, rather than a rotator phase. For C_{40} the liquid-to-rotator transition should be at 80.8 °C, but is preempted by the liquid-to-crystal transition at 80.9 °C [29]. Therefore, in the C_{40}+C_{18}OH mixtures the alkane also freezes into the crystalline phase for almost all ϕ^b studied. For C_{44}, the liquid-to-rotator transition should occur at 84.9 °C, and the liquid-to-crystal transition at 85.5 °C [29]. Here also, almost all concentrations ϕ^b investigated for the C_{44}+C_{22}OH mixture must freeze into the crystalline phase. In conclusion, approach (b) yields a good fit only if we assume that the transition from the liquid phase is into a rotator phase, while the measured transition temperatures for almost all ϕ^b studied in the three mixtures indicate that the transition is into a crystalline phase.

Turning now to approach (c), the phase separation upon freezing dictates using in Eqs. (6) and (7) x_b=1 for the higher molecular weight component and x_b=0 for the lower molecular weight component. As shown by Sirota [30], this eventually leads to an approximately linear behavior of T_b as a function of $\ln(\phi^b)$,

$$T_b \approx T_{b,n} + (k_B T_{b,n}/\Delta S_n^b)\ln(\phi^b), \quad (10)$$

where the subscript n denotes the pure solute alkane component. This behavior holds true for concentrations as low as ϕ^b=0.1. The slope of T_b vs $\ln(\phi^b)$ in Eq. (10) yields ΔS_n^b. If, upon changing ϕ^b, a solid-solid bulk phase boundary is crossed, ΔS_n^b will change. However, T_b will still be linear in $\ln(\phi^b)$ above and below the transition, but the slopes will be different [30]. This linear behavior of T_b vs $\ln(\phi^b)$ is clearly observed for the bulk in Fig. 2.

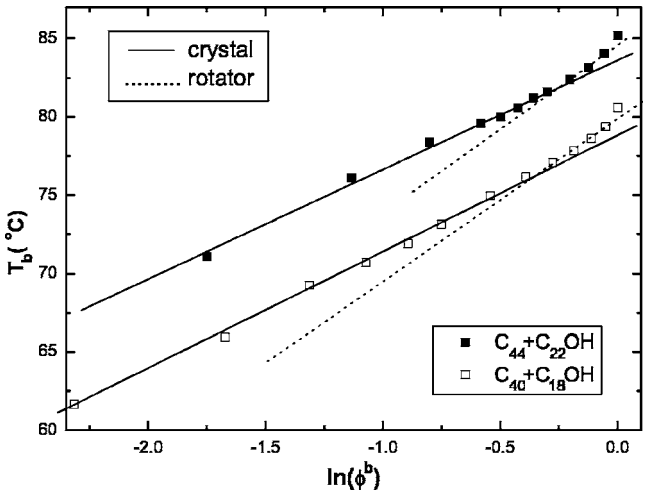

FIG. 2. Measured bulk-freezing temperatures T_b for C_{40}+C_{18}OH melts (open squares) and C_{44}+C_{22}OH melts (solid squares). The slope change at ϕ_t^b indicates a solid-solid phase transition. The freezing temperatures T_b are linear in $\ln(\phi^b)$ both above and below the transition ϕ_t^b as expected for solutions. The fitted lines correspond to the liquid alkane freezing into a rotator (dashed line) or a crystal (solid line) bulk phase.

For all mixtures studied here, the measured T_b values exhibit a slope change for $\phi_t^b \approx 0.7$–0.8, with a linear $\ln(\phi^b)$ dependence below and above it. Using Eq. (10), the entropy change upon freezing was derived from the slopes of the two lines fitted to the $T_b[\ln(\phi^b)]$ values for each mixture [31]. These values, denoted $\overline{\Delta S_n^b}$, are given in Table II, along with literature values for the liquid-to-crystal and liquid-to-rotator

TABLE II. The entropy change upon bulk freezing derived here from the $T_b[\ln(\phi^b)]$ curves $\overline{\Delta S_n^b}$ and from previous calorimetric measurements $\Delta \tilde{S}_n^b$ for the alkanes studied here. ΔS_n^b is the entropy change per unit area and has the units mJ/(m^2 K). $l \to r$ and $l \to x$ indicate liquid-to-rotator and liquid-to-crystal transitions, respectively. The concentration ϕ_t^b, where the solid-liquid transition changes from $l \to r$ to $l \to x$ is determined from the intersection of the different-slope $T_b(\ln \phi^b)$ lines, as shown in Fig. 2.

	$\phi^b > \phi_t^b$ $\overline{\Delta S_n^b}$	$l \to r$ $\Delta \tilde{S}_n^b$	$\phi^b < \phi_t^b$ $\overline{\Delta S_n^b}$	$l \to x$ $\Delta \tilde{S}_n^b$	ϕ_t^b
C_{36}	2.0	2.1	3.5	3.0	0.81
C_{40}	2.4	2.2	3.2	3.4	0.71
C_{44}	2.2	2.4	3.4	3.5	0.78

transitions [3,30], denoted $\Delta\tilde{S}_n^b$. A comparison of the values shows that for $\phi^b > \phi_t^b$, the $\overline{\Delta S_n^b}$ values for all alkanes are within ~10% of the $\Delta\tilde{S}_n^b$ for a liquid-to-rotator transition. We conclude therefore that for $\phi^b > \phi_t^b$ the alkane freezes at T_b into the rotator phase. For $\phi^b < \phi_t^b$ the slope of the fitted line is ~50% lower than at $\phi^b > \phi_t^b$, indicating a corresponding increase in the entropy loss upon freezing. The comparison of the values in Table II reveals a good agreement, again to within ~10% of the $\overline{\Delta S_n^b}$ values with the $\Delta\tilde{S}_n^b$ for a liquid-to-crystal transition. We conclude therefore that for $\phi^b < \phi_t^b$ the alkane freezes at T_b into the crystalline phase.

The intersection of the solid line in Fig. 2 with the T axis at $\phi^b = 1$ yields the temperature at which the liquid-to-crystal transition would have taken place in the pure alkane, if it was not preempted by the liquid-to-rotator transition. These values are between 1 °C and 2 °C lower than the corresponding values obtained from the surface tension measurements. The most probable reason for the small deviations in ΔS^b and T_b are that our freezing points may be slightly supercooled. The deviations could also be due to inhomogeneities in the solutions, or the oversimplified mean-field description used here, which neglects internal degrees of freedom. However, the main features of the bulk behavior are clear: the bulk phase-separates upon freezing into one of two different phases, a rotator phase above ϕ_t^b or a crystalline phase below ϕ_t^b.

B. Results for the surface

For the surface, we tried again the three approaches discussed above, using the measured T_s values as inputs. In approach (a), we use Eqs. (A2) and (A3) and the thermodynamics of mixtures of Appendix A to obtain two equations for $T_s(\phi^s)$. These are analogous to the bulk equations, Eqs. (6) and (7), but with all values being those of the surface, rather than those of the bulk. The fits of these equations to the measured data $T_s(\phi^b)$ could not be done directly, as done for the bulk, since the liquid composition at the surface ϕ^s differs from that of the bulk ϕ^b due to the preferential Gibbs adsorption of the lower-energy bulk species at the surface. However, once ϕ^s was calculated from ϕ^b, using the Gibbs adsorption rule (see Appendix A), fits were done to obtain the value of ω_{cs} and then of x_s by substituting ω_{cs} into the equations for the surface. As in the bulk, no satisfactory fits could be obtained for a finite ω_{cs}, leading to the conclusion that approach (a) does not describe the physics of the system.

Approach (b), which treats both liquid and solid surface phases as strictly regular mixtures [17], new equations, analogous to Eqs. (8) and (9) are derived, and the Gibbs adsorption rule had to be revised from that of approach (a), as shown in Appendix A. Fitting the equations to the T_s data now results in the addition of two new parameters, ω_{lb} and ω_{ls}, to those of approach (a). Good fits are obtained only when using $\omega_{cs} \to \infty$, $\omega_{ls} = 0$, and the fitted ω_{lb} from the bulk fits, which appears in the Gibbs adsorption rule. However, the fit yields ΔS^s values which coincide with the literature values for the liquid-to-rotator transitions for all three liquid mixtures. Moreover, these values do not coincide with the ΔS^s obtained from the slope change upon surface freezing in the measured $\gamma(T)$ curves. From these discrepancies, and from the fact that the fits converge to $\omega_{cs} \to \infty$, we conclude that approach (b) also does not describe the system's behavior well.

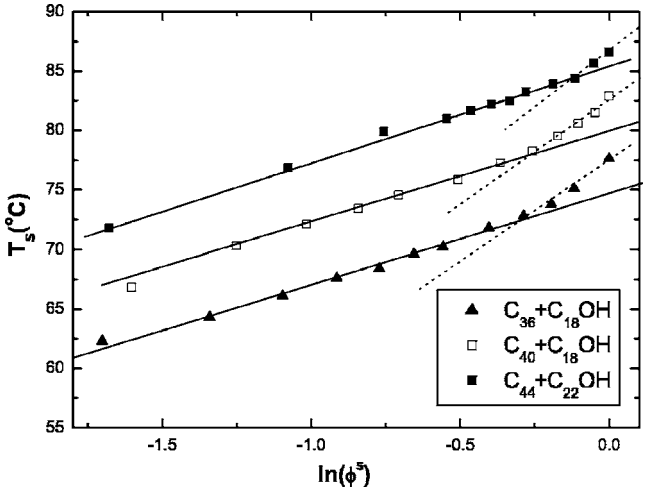

FIG. 3. Measured surface-freezing temperatures T_s for the three mixtures studied. The slope change at ϕ_t^s indicates a solid-solid transition. The freezing temperatures T_s are linear in $\ln(\phi^s)$ both above and below the transition ϕ_t^s as expected for solutions. The fitted lines correspond to the liquid alkane freezing at the surface into a rotator (dashed line) or a crystal (solid line) phase.

In approach (c), the liquid phase is treated as an ideal mixture, which phase separates upon freezing, and thus the solid phase is that of the pure alkane component, i.e., $x_s = 1$ for the alkane and $x_s = 0$ for the alcohol. As for the bulk, this yields [30]

$$T_s \approx T_{s,n} + (k_B T_{s,n}/\Delta S_n^s)\ln(\phi^s). \tag{11}$$

Note that the mole fraction ϕ^s of the liquid-surface phase differs from the mole fraction ϕ^b of the liquid-bulk phase, and has to be calculated from the Gibbs adsorption rule, Eq. (A4). As for Eq. (10), the slope of T_s vs $\ln(\phi^s)$ yields the entropy change upon freezing, ΔS_n^s. In contrast with the bulk, however, this quantity can be obtained independently from the slope change in $\gamma(T)$ at T_s upon the freezing of the surface. The difference between these quantities, however, is that the one derived from Eq. (11) is obtained per mole, or per molecule, while the one derived from $\gamma(T)$ is obtained per unit area. To convert one to the other, knowledge of the area occupied by a molecule at the surface is required. For the ordered solid phase, this can be obtained from the x-ray-derived unit cell dimensions, assuming that the surface is uniformly covered by the crystalline surface monolayer. For the disordered liquid phase this is not possible and a molecular area of 20–25 Å^2/molecule, slightly larger than that of the solid-surface monolayer, is usually assumed.

The measured surface-freezing temperatures T_s and the fits obtained using Eq. (11) of approach (c), are shown in Fig. 3 for the three mixtures studied. As found for the bulk, the surface of all liquid mixtures seems to undergo a phase transition at ϕ_t^s, where the slope changes in Fig. 3. The T_s curves remain linear in $\ln(\phi^s)$ both above and below the

TABLE III. The measured values for $\overline{\Delta S_n^s}$ [in units of mJ/(m^2 K)] upon surface freezing, calculated using approach (c) above and below the phase transition ϕ_t^s.

	$\phi^s > \phi_t^s$ $\overline{\Delta S_n^s}$	$\phi^s < \phi_t^s$ $\overline{\Delta S_n^s}$	ϕ_t^s
C_{36}	1.3	3.2	0.74
C_{40}	1.4	3.2	0.77
C_{44}	1.5	3.1	0.89

transition. The values for the entropy change $\overline{\Delta S^s}$ calculated from Eq. (11) above and below the transition are given in Table III.

Comparing $\overline{\Delta S^s}$ calculated from the fits with the ΔS^s values obtained independently from our surface tension measurements as listed in Table I, reveals that for $\phi^b < \phi_t^s$ the two independently derived values agree well with each other for all three series of the liquid mixtures. These values indicate that the transition at T_s is into a crystalline phase rather than a rotator phase. This is in line with the bulk behavior, and with the fact that T_s is well below the temperature of the pure alkane's bulk transition into the crystalline phase. The x-ray results, discussed below, strongly support this conclusion.

For $\phi^b > \phi_t^s$, the $\overline{\Delta S^s}$ calculated from the fits of Eq. (11) to the measured T_s data are considerably smaller than those obtained from the surface-tension measurements listed in Table I, in some cases by as much as a factor of 2. The change in the ΔS^s values in Table I around ϕ_t^s supports the conclusion that a transition occurs at that concentration. The reduction in $\overline{\Delta S^s}$ indicates that for $\phi^b > \phi_t^s$ the freezing at the surface is into a rotator phase rather than a crystalline phase. Even a lower-than-bulk entropy change can be explained if the rotator phase formed is structurally imperfect. However, the fact that the values derived for the entropy are different for the two types of measurements is not understood. Unlike for $\phi^b < \phi_t^s$, for $\phi^b > \phi_t^s$ x-ray diffraction did not reveal any peaks, and thus the in-plane order, if any, could not be determined. Further studies are needed to resolve this discrepancy.

IV. RESULTS: STRUCTURE

The values obtained in both XR and GID measurements for the surface-normal and the surface-parallel structure of the surface-frozen layer are listed in Table IV, and are discussed in detail in the following subsections.

A. Surface-normal structure

The Fresnel-normalized x-ray reflectivities measured for several $C_{44}+C_{22}OH$ mixtures in their surface-frozen phase are shown in Fig. 4. All reflectivities measured for $T > T_s$ exhibit a monotonic decrease, typical of a liquid surface having a Gaussian roughness due to thermally-induced capillary waves [3]. When cooled to below T_s, all R/R_F curves, including those in Fig. 4, show Kiessig-type fringes, indicating the existence of a surface layer with an electron density different from that of the underlying bulk. The thickness of the surface-frozen layer D is related to the period Δq_z of these fringes by $D \approx 2\pi/\Delta q_z$. In all three series of melts, $C_{36}+C_{18}OH$, $C_{40}+C_{18}OH$, $C_{44}+C_{22}OH$, the thickness of the surface-frozen layer remained almost constant and independent of ϕ^b, as shown by the almost equal fringe periods of the R/R_F curves in Fig. 4. The slight changes in the fringe periods result from variation of the molecular tilts with ϕ^b, as discussed below.

Even though the thermodynamical results discussed above strongly support the conclusion that the surface-frozen layer is an alkane monolayer, we have also explored the possibility that the surface-frozen phase is a bilayer of alcohol molecules. Accordingly, two models were used in the XR fits of Eq. (1): a two-slab model ($N=2$) describing the alkane monolayer and a four-slab model ($N=4$) describing the alcohol bilayer, as discussed above. The fits of the four-slab model did not provide any improvement over those of the two-slab model [lines in Fig. 4(a)]. Moreover, the bilayer (four-slab) model includes a narrow slab at the bilayer's center, the density of which is higher than that of the adjacent alkyl chains' slabs. This slab corresponds to the layer of the denser hydroxyl groups. In the four-slab model fits the density of this slab refined very close to that of the alkyl chains' slabs, resulting in an effective density profile indistinguishable from that of the two-slab model on the scale of Fig. 4(a). Thus, the two-slab model seems to be the simplest model that fits the measured R/R_F curves well. The thickness values obtained from the fits are listed in Table IV, and well agree with those expected for extended alkanes. In all density profiles in Fig. 4(b) the density of the $(CH_2)_{n-2}$ layer was found to be $0.31 \pm 0.007 e/\text{Å}^3$. All roughness values were equal to 4.2 ± 0.4 Å^3. No systematic variations with temperature (within the limited temperature range of existence, $\Delta T = T_s - T_b$) or bulk concentration, were observed for the layer thickness and density. This lends further support to the conclusion, derived above from the thermodynamical measurements and discussion that the binary melts must be treated as ideal solutions rather than mixtures with the alkane freezing out at the surface.

B. Surface-parallel structure

The in-plane order was explored by GID measurements. The q_r positions of the diffraction peaks yield information on the crystalline packing, while the q_z intensity distribution (BR) yields information on the azimuthal direction and magnitude of the molecular tilt from the surface normal [26,32,33]. The measured GID patterns and the corresponding BRs for two different concentration $C_{44}+C_{18}OH$ mixtures are shown in Fig. 5, along with fits of the GID peaks by Gaussians and of the BRs by Eq. (3). The various quantities derived from the GID and BR fits for the three mixtures studied here are listed in Table IV. Note that GID peaks (and thus also BR distributions) were observed only for $\phi^b < \phi_t^s$, where the thermodynamical analysis of $T_s[\ln(\phi^b)]$ above indicated the existence of a crystalline surface phase rather than a rotator surface phase. For $\phi^b > \phi_t^s$, no GID peaks were observed for any of the mixtures studied here.

TABLE IV. XR-, GID-, and BR-derived quantities. D is the layer thickness as obtained from the XR measurements, (q_r^p, q_z^p) are the GID and BR peak positions, and θ is the molecular tilt. All tilts are in the NNN (next-nearest-neighbor) direction, unless specified otherwise.

ϕ^b	D (Å)	q_r^p (Å^{-1})	q_z^p (Å^{-1})	θ (°)
		$C_{36}(\phi^b)+C_{18}OH(1-\phi^b)$		
0	48.84	1.50	0.1	<5[a]
0.319	44.52			
0.445	44.56			
0.814	42.72			
0.914	42.73			
1	42	1.496	0.0	18[b]
		1.496	0.39	
		$C_{40}(\phi^b)+C_{18}OH(1-\phi^b)$		
0	48.8	1.50	0.1	<5[a]
0.188	48.8	1.48	0.2	14
0.342	48.4			
0.472	46.5	1.486	0.3	20
0.581	47.2	1.475	0.3	21
		1.55	0.6	
0.829	46.6			
0.892	46.8			
0.949	46.6			
1	46.8	1.489	0.0	21[b]
		$C_{44}(\phi^b)+C_{22}OH(1-\phi^b)$		
0	58.3	1.50	0.1	<5[a]
0.174	51.8	1.487	0.3	21
		1.573	0.5	
0.322	51.7	1.483	0.3	22
0.558	51.3	1.472	0.3	24
0.699	50.0	1.473	0.3	24
		1.51	0.7	
0.816	49.5	1.473	0.7	25
0.883	50.9			
1	50.3	1.476	0.356	26
		1.476	0.740	

[a]The surface-frozen phase is an untilted alcohol bilayer.
[b]Tilt is towards nearest neighbors (NN).

As can be observed in Table IV, for some mixtures, e.g., $\phi^b=0.174$ and 0.699 of $C_{44}+C_{22}OH$, two GID peaks were found, peaking at different q_z^p of the BR, as shown in Fig. 5. The two GID peaks imply a rectangular unit cell of dimensions $b \neq \sqrt{3}a$. The BR peak positions $q_{z_2}^p = 2q_{z_1}^p \neq 0$ indicate that the molecules are tilted from the surface normal in the next-nearest-neighbor direction, as discussed in Sec. II above [33]. The fits of all mixtures showing two peaks could be indexed in a unit cell $a_\perp = 5.0 \pm 0.1$ Å and $b_\perp = 7.5 \pm 0.2$ Å, where $a_\perp$ and $b_\perp$ are the unit-cell dimensions in the plane perpendicular to the molecular long axis. For our tilt direction these values are related to the unit-cell dimensions in the surface plane by $a_\perp = a$ and $b_\perp = b \cos\theta$. The different molecular tilt angles for the different mixtures result in different unit cell dimensions a and b, in spite of the common $a_\perp$ and $b_\perp$. The unit cell dimensions, and, in particular, the fact that $b_\perp < \sqrt{3}a_\perp$, imply that the chains form a herringbone packing (see Fig. 13 in Ref. [33]). The x-ray derived area per molecule, $A_x = 18.8$ Å^2/molecule is also typical of a herringbone packing and would be too small for a rotator phase, where the molecular area is ~ 20 Å^2/molecule. We conclude therefore that for the mixtures where two GID peaks are observed, the packing is herringbonelike with two molecules per unit cell. Note that the packing of the surface-frozen layer of the monocomponent ($\phi^b = 1$) alkanes used here differs from that of the mixtures. The surface-frozen monolayers of C_{36} and C_{40} are hexagonally-packed rotator phases, with a nearest-neighbor tilt direction. The surface-frozen monolayer at the

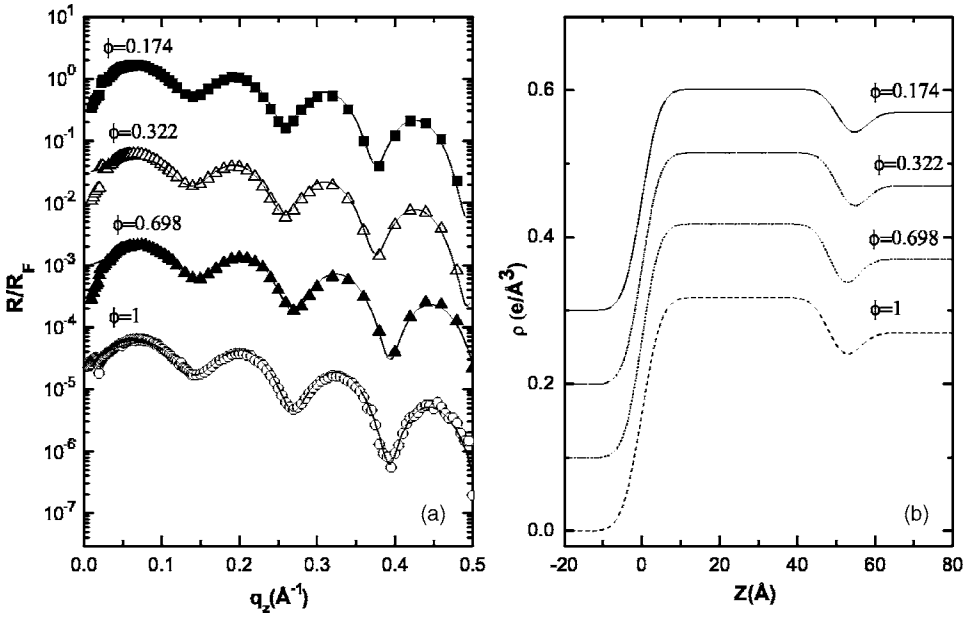

FIG. 4. (a) Measured (points) and model-fitted (lines) x-ray reflectivity curves, for the surface-frozen phase of the $C_{44}(\phi^b)+C_{22}OH(1-\phi^b)$ melts, normalized to the Fresnel reflectivity of an ideal surface. The fringe period is inversely proportional to the surface-frozen monolayer's thickness, which is observed to remain almost constant for all concentrations of C_{44}. (b) The surface-normal electron-density profiles derived from the fits in (a). The reflectivities and density profiles are shifted vertically, for clarity.

surface of pure C_{44} has a herringbone packing and a next-nearest-neighbor tilt, same as the mixtures discussed above. However, it has an hexagonal packing in the surface plane [3], so that only a twice-degenerate single GID peak is observed, exhibiting two BR peaks at $q^p_{z_2}=2q^p_{z_1}\neq 0$.

In several mixtures only one GID peak was observed (see Table IV), with a single BR peak at $q^p_z\neq 0$. However, as the values in Table IV show, the q^p_r positions of these peaks, as well as their BR q^p_z peaks, almost coincide with those of the lowest-q_r (and more intense) peaks of the liquid mixtures where two peaks were observed. We have therefore assumed that the structure of the single-GID-peak monolayers is the same as that of the two-GID-peak monolayers. The absence of the higher-q_r peak could be due to the coarse-grained powder consistency of the monolayer, which does not always provide properly oriented crystallites for observing all reflections without an azimuthal rotation of the sample [34]. In addition, the higher q_r also results in a greater reduction in the peak intensity by the Debye-Waller factor. Similar peak suppression was observed in other mixtures and pure compounds exhibiting surface freezing [3,4,10–12], and in Langmuir films on aqueous and liquid-mercury subphases.

Under this assumption, the analysis of the BR resulted in a next-nearest-neighbor tilt, and a molecular tilt following the trend set by the liquid mixtures showing two peaks. The entropy change upon surface freezing (ΔS) (see Table I) obtained in the surface tension measurements and in the thermodynamical analysis of the measured $T_s[\ln(\phi^b)]$ values discussed above, also support the conclusion of a herringbone-packed crystalline phase for both the one-GID-peak and two-GID-peak monolayers, since all are obtained for $\phi^b<\phi^s_t$. As can be observed in Table IV, the molecular tilt θ was found to increase with alkane concentration for all mixtures where this quantity could be derived from the measurements. While the magnitude of this effect is not large, especially for $C_{44}+C_{22}OH$, it seems to be systematic. We speculate that this

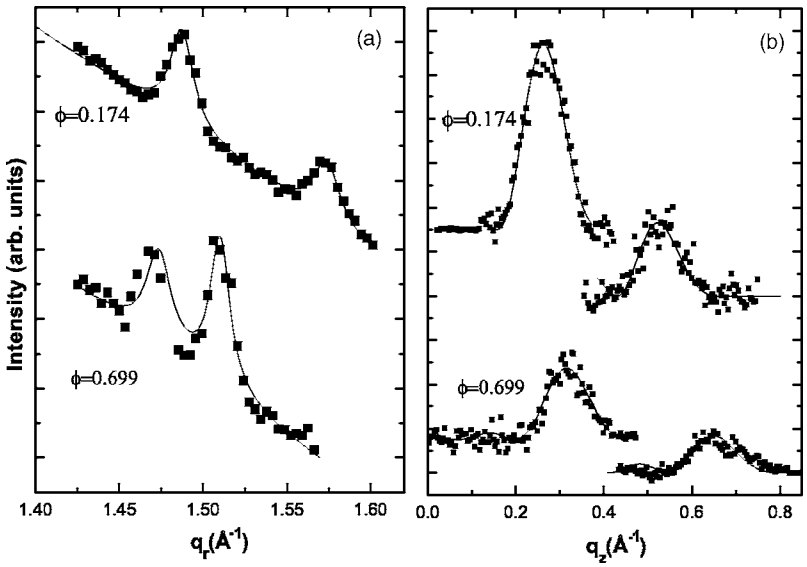

FIG. 5. The (a) GID and (b) BR patterns measured (points) for $C_{44}(\phi^b)+C_{22}OH(1-\phi^b)$ mixtures. The lines in (a) are a phenomenological fit by one Gaussian per peak plus a linear background. The lines in (b) are fits by the model discussed in the text.

effect may arise from the incorporation of a very small number of alcohol molecules into the SF layer. These foreign molecules are effectively impurities, in that they induce defects which favor a less-tilted phase compared to the pure alkane layer. Under this scenario, the defect density increases with bulk alcohol concentration, consistent with the observed trends in the tilt and layer spacing of the surface-frozen layer.

We have also attempted to fit the GID and BR data assuming that the surface phase is a bilayer of alcohol molecules [4]; however, the fits were rather poor, further supporting the conclusion that the surface phase is an alkane monolayer. Models using a layer consisting of both alcohol and alkane molecules also failed to provide a good agreement with the measured GID and BR curves.

For $\phi^b > \phi_t^s$, no GID peaks were observed for any of the mixtures studied, despite the large value of the corresponding ΔS, which may be taken to suggest a transition to an ordered surface-frozen phase. This may result from a very small coherence length for the monolayer's in-plane structure. A high concentration of defects may further reduce the range of the order. A short coherence length (a few tens of Å in our case) results in the GID peaks becoming low and broad to the limit of being indistinguishable above the background. A short coherence length is in line with the conclusion, derived from the $T_s[\ln(\phi^b)]$ data above, that for $\phi^b > \phi_t^s$ the surface phase is a rotator phase. An example of a dramatic reduction in the in-plane coherence length of densely-packed alkyl chains upon transition from a crystalline herringbone packing to a rotator packing was recently observed by surface-coverage-dependent GID measurements in mercury-supported Langmuir films of stearic acid [35]. The lower-than-bulk $\overline{\Delta S^s}$ values obtained for the surface phase for $\phi^b > \phi_t^s$ also support the assumption of a high concentration of defects, as discussed above.

V. CONCLUSION

The measurements presented here for alkane-alcohol mixtures with a mismatch of $0 \leqslant \Delta n \leqslant 4$ between the carbon numbers of the alkane $(2n)$ and twice that of the alcohol (n) reveal that surface freezing occurs in these mixtures at all concentrations. However, the surface-frozen layer is always nearly a pure alkane monolayer. The behavior of the mixtures is found to be that of a solution, which phase-separates upon freezing, both in the bulk and at the surface. The liquid-solid freezing transition occurs to a crystalline phase for concentrations $\phi^{b,s} < \phi_t^{b,s} \approx 0.8 \pm 0.1$ for all mixtures studied here, for both bulk and surface. The surface phase is herringbone-packed with concentration-dependent molecular tilts in the next-nearest-neighbor direction. For $\phi^{b,s} > \phi_t^{b,s}$ the entropy change upon freezing indicates that the frozen phase both at the surface and in the bulk is a rotator phase. However, as no x-ray GID peaks were observed in this phase for any of the mixtures studied, this conclusion could not be verified independently. An unresolved discrepancy was found between the values of the entropy loss upon surface freezing derived from the freezing temperatures and that derived from the surface-tension measurements. However, the entropy change upon bulk freezing derived from the bulk-freezing temperatures agrees well with published, calorimetrically measured, values. Thus, the behavior of the mixtures, both thermodynamically and structurally, is well understood for $\phi^{b,s} < \phi_t^{b,s}$. The same holds for the bulk for $\phi^b > \phi_t^b$. The elucidation of the surface behavior for $\phi^s > \phi_t^s$ requires further studies.

The fact that no simple mixed alkane-alcohol surface-frozen phases were observed indicates that the repulsion between the polar hydroxyl groups of the alcohols and the adjacent alkyl chains of the alkanes would be prohibitively high for a random (or even nonrandom) mixing of the two species within the surface-frozen phase. The likelihood for such packing is highest for Δn being close to zero, since this minimizes the repulsion between the alkyl moieties of the two species due to length mismatch. Choosing longer alkanes and alcohols for future studies may yield a mixture-like, rather than solutionlike, behavior, since such choice increases the van der Walls chain-chain interaction, while the hydroxyl-alkyl repulsion of adjacent molecules remains the same. However, the fact that the surface freezing was not observed in alkane molecules longer than 52 carbons limits the choices, as does the fact that for carbon numbers of 44 and up, the packing of the surface-frozen layer is the more restrictive herringbone crystalline packing rather than the less dense rotator packing.

ACKNOWLEDGMENTS

Beamtime at beamline X22B, NSLS, Brookhaven National Laboratory is gratefully acknowledged. Brookhaven National Laboratory is supported by the U.S. Department of Energy under Contract No. DE-AC02-98CH10886.

APPENDIX: THERMODYNAMICS OF MIXTURES

The behavior of the surface phase of a mixture of chain molecules can generally be accounted for using properties of pure components and taking into consideration the mixing entropy and molecular interactions [17,18]. Three approaches were discussed above for dealing with the thermodynamics of the bulk and surface in the liquid and crystalline phases. The most general free energy, which covers all phases discussed under these approaches, is given by

$$F^{pq} = N f_n^{pq} + M f_m^{pq} + k_B T \left[N \ln \frac{N}{N+M} + M \ln \frac{M}{N+M} \right] + \omega_{pq} \frac{NM}{N+M}. \tag{A1}$$

Here, N and M are the number of C_n and C_m molecules in the mixture, respectively, $f_i^{pq} = \varepsilon_i^{pq} - TS_i^{pq}$ is the free energy per molecule in pure C_i $(i=n,m)$ in the liquid or crystalline $(p=l,c)$ phase, at the surface or in the bulk $(q=s,b)$. ε and S are, respectively, the energy and entropy per molecule in this phase. The third term is the mixing entropy, and the last term is the repulsion energy, due to the length mismatch of the molecules. The magnitude of this term is given by the interchange parameter ω_{pq}, half the energy cost of exchanging two molecules, each coming from different pure samples,

with one another [17,18]. The intermolecular repulsion term is given, therefore, by ω_{pq} times the probability of a nonidentical pair occurring in the binary mixture, neglecting higher-order interactions.

At a liquid/solid transition T_q the solid crystal phase coexists with the liquid phase. Thus, at T_q each component must have the same chemical potential in both phases: $\mu_n^l(T_q)=\mu_n^c(T_q)$ for C_n (where $\mu_n^p=\partial F^p/\partial N$), and a similar expression for C_m. This yields

$$f_n^{lq} + k_B T \ln \phi^q + \omega_{lq}(1-\phi^q)^2 = f_n^{cq} + k_B T \ln x_q + \omega_{cq}(1-x_q)^2, \tag{A2}$$

$$f_m^{lq} + k_B T \ln(1-\phi^q) + \omega_{lq}(\phi^q)^2 = f_m^{cq} + k_B T \ln(1-x_q) + \omega_{cq} x_q^2. \tag{A3}$$

Here ϕ^q is the mole fraction of C_n molecules in the liquid phase [with $\phi^b=N/(N+M)$] and x_q is the mole fraction of the same molecules in the crystal phase. It is important to note that, in general, the crystal phase composition x_q differs from the liquid-phase composition ϕ^b. Moreover, the liquid-phase composition in the bulk ϕ^b differs from that at the surface ϕ^s due to the enrichment of the surface by the low-surface-tension species, according to the Gibbs adsorption rule (see below). The same-phase interchange energy of the bulk is different, in general, from that of the surface. The same holds for the different-phase interchange energies at the surface or in the bulk. The free-energy difference in the liquid and crystal bulk phases is calculated, for each component, as $f_i^{cq}-f_i^{lq}=(T-T_{q,i})(S_i^{lq}-S_i^{cq})=(T-T_{q,i})\Delta S_i^q$, where ΔS_i^q is the entropy change per molecule of a pure C_i sample at its freezing temperature $T_{q,i}$ $(i=n,m)$.

Equation (A3) is used to obtain Eqs. (6)–(10) for the bulk $T_b(\phi^b)$ and their equivalents for the surface $T_s(\phi^b)$ for the three approaches discussed in the text. In approach (a), the liquid phase is considered to be an ideal mixture, so that ω_{lq} is set to zero, while the crystalline phase is a strictly-regular mixture [17] with $\omega_{cq}\neq 0$. In approach (b) both liquid and solid phases are strictly regular mixtures with $\omega_{lq}\neq 0$ and $\omega_{cq}\neq 0$. In approach (c) the liquid is ideal, with ω_{lq} set to zero. The liquid is assumed to phase separate upon freezing, so that both the repulsion and the mixing entropy terms are taken to be zero, as there is no mixing between the species. These different choices lead to the different expressions for the freezing temperatures T_q in the discussion in the text.

As mentioned above, the liquid composition at the surface ϕ^s differs from that of the bulk ϕ^b due to the Gibbs adsorption rule [18]. ϕ^s can be readily calculated from ϕ^b by using the chemical potentials of the liquid bulk and surface phases, as given in Eqs. (A2) and (A3) above, with standard thermodynamics [10,17,36,38]

$$\phi^s = \phi^b \Gamma_t / (1-\phi^b+\phi^b\Gamma_t), \tag{A4}$$

where the dimensionless parameter Γ_t is defined as

$$\Gamma_t = \exp[(\gamma_m-\gamma_n)A/k_BT]. \tag{A5}$$

γ_n is the surface tension of the pure alkane component at a fixed temperature $(T=\text{const}>T_{s,n})$ taken from previous studies [1,3,11]. γ_m is the surface tension of the alcohol component, at the same T, also taken from previous studies [12,37]. A is the area per molecule [10], estimated as $A\approx 25$ Å^2. Thus, Eq. (A4) leads, in our case, to a slight enrichment of the surface by alcohols, so that $\phi^b \gtrsim \phi^s$. The difference between ϕ^b and ϕ^s is small and continuous, so that the general phase behavior of the surface is close to that of the bulk.

In the case of a nonideal mixture, the chemical potentials of the liquid, on the surface and in the bulk, are different from those used to calculate Eq. (A4). When these changes are taken into account, ϕ_s changes and is given by

$$\frac{\phi^s}{1-\phi^s}\exp[(1-2\phi^s)\omega_{ls}] = \Gamma_t \frac{\phi^b}{1-\phi^b}\exp[(1-2\phi^b)\omega_{lb}]. \tag{A6}$$

Using published values for the various quantities of the pure components [1–4], and the Gibbs rule to relate ϕ^s to ϕ^b, Eqs. (A2) and (A3) can be solved for the surface phases by fits to the measured T_s values. The different interchange parameters, and x_s, can then be calculated, as done for the bulk [11,12].

[1] X. Z. Wu, E. B. Sirota, S. K. Sinha, M. Deutsch, B. H. Cao, and M. W. Kim, Science **261**, 1018 (1993).

[2] X. Z. Wu, E. B. Sirota, S. K. Sinha, B. M. Ocko, and M. Deutsch, Phys. Rev. Lett. **70**, 958 (1993).

[3] B. M. Ocko, X. Z. Wu, E. B. Sirota, S. K. Sinha, O. Gang, and M. Deutsch, Phys. Rev. E **55**, 3164 (1997).

[4] O. Gang, X. Z. Wu, B. M. Ocko, E. B. Sirota, and M. Deutsch, Phys. Rev. E **58**, 6086 (1998).

[5] J. W. M. Frenken and J. F. van der Veen, Phys. Rev. Lett. **54**, 134 (1985); H. Dosch, T. Höfer, J. Peisl, and R. L. Johnson, Europhys. Lett. **15**, 527 (1991); D. M. Zhu and J. G. Dash, Phys. Rev. Lett. **57**, 2959 (1986); M. Elbaum and M. Schick, *ibid.* **66**, 1713 (1991); E. A. Jagla, S. Prestipino, and E. Tosatti, *ibid.* **83**, 2753 (1999); Y. Fukaya and Y. Shigeta, *ibid.* **85**, 5150 (2000); X. Wei, P. B. Miranda, and Y. R. Shen, *ibid.* **86**, 1554 (2001).

[6] J. C. Earnshaw, and C. J. Hughes, Phys. Rev. A **46**, R4494 (1992).

[7] O. Gang, B. M. Ocko, X. Z. Wu, E. B. Sirota, and M. Deutsch, Phys. Rev. Lett. **80**, 1264 (1998).

[8] E. Sloutskin, H. Kraack, B. M. Ocko, J. Ellman, M. Möller, P. LoNostro, and M. Deutsch, Langmuir **18**, 1963 (2002).

[9] X. Z. Wu, B. M. Ocko, H. Tang, E. B. Sirota, S. K. Sinha, and M. Deutsch, Phys. Rev. Lett. **75**, 1332 (1995).

[10] E. Sloutskin, E. B. Sirota, H. Kraack, B. M. Ocko, and M. Deutsch, Phys. Rev. E **64**, 031708 (2001).

[11] E. Sloutskin, X. Z. Wu, T. B. Peterson, O. Gang, B. M. Ocko, E. B. Sirota, and M. Deutsch, Phys. Rev. E **68**, 031605 (2003).

[12] E. Sloutskin, O. Gang, H. Kraack, A. Doerr, E. B. Sirota, B. M. Ocko, and M. Deutsch, Phys. Rev. E **68**, 031606 (2003).

[13] K. S. Gautam and A. Dhinojwala, Phys. Rev. Lett. **88**, 145501 (2002); S. Prasad *et al.*, Macromolecules **38**, 2541 (2005).
[14] Z. Dogic, Phys. Rev. Lett. **91**, 165701 (2003).
[15] S. Prasad and A. Dhinojwala, Phys. Rev. Lett. **95**, 117801 (2005).
[16] P. Huber, V. P. Soprunyuk, J. P. Embs, C. Wagner, M. Deutsch, and S. Kumar, Phys. Rev. Lett. **94**, 184504 (2005).
[17] E. A. Guggenheim, *Mixtures* (Oxford University Press, Oxford, 1952).
[18] J. H. Hildebrand and R. L. Scott, *The Solubility of Nonelectrolytes* (Reinhold, New York, 1966).
[19] E. Sloutskin, E. B. Sirota, O. Gang, X. Z. Wu, B. M. Ocko, and M. Deutsch, Eur. Phys. J. E **13**, 109 (2004).
[20] G. L. Gaines, *Insoluble Monolayers at Liquid Gas Interface* (Wiley, New York, 1966); G. Roberts, *Langmuir-Blodgett Films* (Plenum Press, New York, 1990).
[21] M. K. Sanyal, S. K. Sinha, K. G. Huang, and B. M. Ocko, Phys. Rev. Lett. **66**, 628 (1991).
[22] When the slope change in $\gamma(T)$ is not sharp, e.g., for $\phi=0.655$ in Fig. 1, T_s is taken as the abscissa of the intersection point of the extensions to the T_s region of the low- and high-temperature linear sections of $\gamma(T)$.
[23] J. Als-Nielsen and D. McMorrow, *Elements of Modern X-Ray Physics* (Wiley, New York, 2001).
[24] M. Deutsch and B. M. Ocko, *Encyclopedia of Applied Physics*, edited by G. L. Trigg (VCH, New York, 1998), Vol. 23, p. 479.
[25] I. M. Tidswell *et al.*, Phys. Rev. B **41**, 1111 (1990).
[26] J. Als-Nielsen and K. Kjaer, *Phase Transitions in Soft Condensed Matter*, edited by T. Riste and D. Sherrington (Plenum Press, New York, 1989), p. 245.
[27] G. H. Vineyard, Phys. Rev. B **26**, 4146 (1982).
[28] M. L. Schlossman and P. S. Pershan, *Light Scattering by Liquid Surfaces and Complementary Techniques*, edited by D. Langevin (Dekker, New York, 1990).
[29] H. Kraack, E. B. Sirota, and M. Deutsch, J. Chem. Phys. **112**, 6873 (2000).
[30] E. B. Sirota, J. Chem. Phys. **112**, 492 (2000).
[31] The points at $\phi=1$ of the three mixtures were excluded from the liquid-to-rotator line fits, since pure C_{40} and C_{44} freeze into a crystalline phase rather than a rotator phase, and even though pure C_{36} freezes into a rotator phase, this may differ from the rotator phase of a mixture.
[32] D. K. Schwartz, M. L. Schlossman, and P. S. Pershan, J. Chem. Phys. **96**, 2356 (1991).
[33] V. M. Kaganer, H. Möhwald, and P. Dutta, Rev. Mod. Phys. **71**, 779 (1999).
[34] The experimental setup allowed only a very limited rotation of the trough relative to the incident beam's direction.
[35] H. Kraack, B. M. Ocko, P. S. Pershan, E. Sloutskin, and M. Deutsch, Science **298**, 1404 (2002).
[36] R. Defay, I. Prigogine, A. Bellemans, and D. H. Everett, *Surface Tension and Absorption* (Wiley, New York, 1966).
[37] S. S. Katti and S. Pathak, J. Chem. Eng. Data **14**, 73 (1969).
[38] L. E. Reichl, *A Modern Course in Statistical Physics* (University of Texas Press, Austin, 1980).